

# Graphene Nanocutting Through Nanopatterned Vacancy Defects

Rhonda Jack<sup>1,2</sup>, Dipanjan Sen<sup>1,3</sup>, and Markus J. Buehler<sup>1,\*</sup>

<sup>1</sup>Laboratory for Atomistic and Molecular Mechanics (LAMM), Department of Civil and Environmental Engineering, Massachusetts Institute of Technology, 77 Mass. Ave., Room 1-235A&B, Cambridge, MA, 02139, USA

<sup>2</sup>Department of Chemical Engineering, Hampton University, Hampton VA, USA

<sup>3</sup>Department of Materials Science and Engineering, Massachusetts Institute of Technology, 77 Mass. Ave., Cambridge, MA, 02139, USA

The recent discovery of single graphene sheets and the remarkable technologies envisioned for graphene-based materials necessitate the ability to assemble and reproduce nano-precise graphene structures. Here we demonstrate an approach to create atomically precise single graphene structures by applying tensile load to single sheets of graphene that feature specific patterns of vacancies. We report a computational nanoengineering approach that utilizes the first principles based reactive force field potential (ReaxFF), applied here to simulate the fracture mechanics of up to 40,000 fully reactive atoms. We find that the direction and dynamical behavior of graphene fracture can be controlled by the presence of atomistic defects in the form of atomic vacancies placed throughout the sheet. We find that these vacancies produce distinct effects on the resulting fracture surface geometries, defined by the specific patterns in which they occur throughout the 2D structure. For instance, we are able to cut graphene sheets along controlled zigzag patterns on the nanoscale using specific arrangements of vacancies. These findings suggest novel possibilities aimed at cutting and producing atomically precise graphene structures, enabling advances in graphene nanotechnology. The study reported here is the first to apply ReaxFF to model fracture of graphene sheets.

**Keywords:** Graphene, Fracture, Materials Failure, Reactive Force Field, Nanoengineering, ReaxFF, Vacancy.

## 1. INTRODUCTION

Until recently, graphene was considered to be primarily an academic concept, since calculations suggested that it was thermodynamically impossible to synthesize single sheets of graphene.<sup>1</sup> However, since the successful isolation of single sheets of graphene in 2004 by Geim and his colleagues,<sup>2</sup> there have been a remarkable advances in the way scientists utilize 2D materials such as graphene.<sup>1</sup> These materials could find applications in novel nanoelectronics devices, due the variety of possibilities that these unique electronic properties of 2D graphene provide.<sup>3,4</sup> The unique properties of graphene, relative to other conductive materials, are a result of the distinctive energy band structure characteristic of this material.<sup>5</sup> Applications of graphene could include the synthesis of graphene nanocomposites, graphene powder for use in electric batteries, solid state gas sensors and hydrogen storage

devices, and even the possibility of room temperature ballistic transistors,<sup>6</sup> among others. A quite promising avenue of graphene nanotechnology is described in the broad realm of graphene based nanoelectronic devices,<sup>7</sup> and it has been suggested that this material may play a crucial role in the post-silicon world.

For the successful development of such nanoelectronic devices, there is one particularly important challenge that must be overcome, in order to enhance the ability to provide better control the electronic activity of graphene<sup>8,9</sup> (e.g., in order to engineer appropriate band gap structures<sup>10</sup>). A proposed method of designing these band gaps is to arrange the graphene sheet in geometrically confined patterns of very narrow ribbons called graphene nanoribbons (GNRs), which confine the electron movement laterally along the ribbons. Previous work has shown that the size of the band gap is inversely proportional to the size of the ribbon.<sup>11–13</sup> Based on the band gap size required for room temperature electronic devices, the size of the graphene ribbons required is on the order

\*Author to whom correspondence should be addressed.

of nanometers.<sup>9,14</sup> Furthermore, the need to attain precise reproducibility of the geometry of ribbons is of high priority, and therefore the capacity to manipulate graphene structures at the nano level is considered elementary to facilitate the further development of this technology.

Electron-beam lithography is one of the methods currently used to create GNRs. However, there are limits to the size that this option could provide, where the smallest width achieved thus far are of the order of tens of nanometers.<sup>15</sup> Recently, researchers proposed a method of cutting graphene by using Ni nanoparticles, providing a high-precision chemical “knife.”<sup>16</sup> Another method that was recently proposed is the use of Scanning Tunneling Microscopy (STM),<sup>17</sup> which enables one to achieve the desired ribbon sizes that make it possible to create room temperature graphene electronic devices. However, some of these options (e.g., the use of STM) are limited by experimental difficulties and the high cost that such a high throughput strategy would incur.

Here we propose an alternative approach to create graphene nanostructures with specific dimensions, with structural precision at the nano-scale. Our method is based on introducing atomic-level defect patterns in graphene, used in conjunction with application of mechanical load. Failure of the defect-patterned graphene sheet occurs following the defect pattern geometry, and thereby generates new surfaces with a particularly designed structure. This approach of inducing fracture along paths of atomic-level defects is based on the deliberately weakening of the graphene structure. This approach might, with further experimental and technological development, result in the development of a time- and cost-efficient mechanism of producing graphene structures with atomistic precision.

## 2. COMPUTATIONAL APPROACH

Fracture of graphene sheets under tension has been previously studied using Brenner bond-order potential<sup>18</sup> and QM/MM multiscale studies using a combination of *ab initio* methods and Brenner potentials.<sup>19</sup> The computational approach used in the present study is based on the first principles based reactive force field potential ReaxFF, which reproduces results of comparable accuracy to that of a quantum mechanics approach and still offers relatively low computational cost.<sup>20–22</sup> This model is capable of simulating the interaction of the atoms and their bonding as well as reactive systems of up to approximately 40,000 atoms.<sup>23</sup> Earlier applications of ReaxFF in studies of fracture of silicon provided excellent agreement between theory and simulation.<sup>24,25</sup> Further studies focused on the mechanics of carbon nanotubes showed agreement of ReaxFF with earlier computational analysis and experimental studies.<sup>26</sup>

Here we consider a single graphene sheet with a surface crack for seed of mechanical failure (through providing

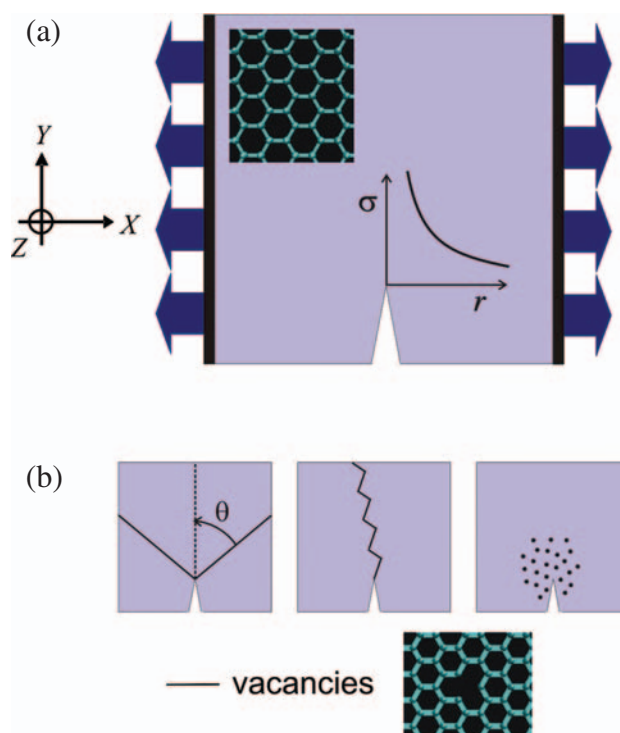


**Fig. 1.** Subplot (a): Geometry of simulation setup of the single graphene sheet with edge crack (crystal orientation shown in inset). Subplot (b) shows the different cases of vacancy patterns studied here, including lines of point different at varying angles, a zig-zag pattern of vacancy defects, and a random placement of vacancies. The crystal snapshot in the lower right corner displays the atomistic details of the vacancy structure, obtained by removing a C atom.

a concentration of stresses at the atomic level), as shown in Figure 1(a). The orientation of the graphene sheet is such that C–C bonds lie parallel to the direction of loading (see inset displayed in Fig. 1(a)). The initial crack is created by removing carbon atoms within a specified region of the perfect sheet, forming a wedge-like initial crack geometry. The system dimensions are  $W = 129 \text{ \AA}$ , and  $H = 151 \text{ \AA}$ , with an initial crack length of  $41 \text{ \AA}$ . The dimensions of the initial crack are determined by considering that the cracks should have a large aspect ratio, but should not be too narrow so as to allow the crack to close up due to interactions across the crack. An *NVT* ensemble dynamics with Berendsen thermostat is used for time integration in the molecular dynamics algorithm, with all runs carried out at a low temperature of 20 K. The single graphene sheets studied in this paper consists of up to 12,000 ReaxFF atoms. The calculations performed with the system are carried out in a parallelized simulation environment, where multiple processors are used to solve the equations of motion. This is achieved by using the General Reactive Atomistic Simulation Program (GRASP) simulation code. Visualization is carried out by using the Visual Molecular Dynamics (VMD) tool.<sup>27</sup>

Vacancies in graphene sheets introduces points of structural weakness.<sup>28</sup> This structural weakening is used here

as a means to control the mechanism of crack propagation. We hypothesize that by introducing distinct patterns of vacancies in the domain ahead of the crack we can direct crack propagation along specific patterns and thereby control the shape of graphene surfaces generated. Several geometries of vacancy defect patterns are depicted in Figure 1(b). The vacancies are introduced in the structure by removing atoms from the graphene lattice as shown in the inlay.

Tensile strain is applied by fixing the three outermost columns of atoms to the left and right of the sheet, then applying a fixed displacement rate on each side, directed away from the sheet and perpendicular to the crack plane, for both types of systems, defected and undefected (resembling mode I loading). The strain rate is fixed at  $1 \times 10^{11}$  1/sec for all simulations reported in this paper.

### 3. COMPUTATIONAL RESULTS

We first report results of the calculations of the reference case, a system without any defects. Figure 2 depicts the dynamics of crack propagation in this system. It is observed that the crack extends almost straight from its initial orientation until the entire specimen is fractured.

We proceed with a discussion of the results that involve vacancy defect structures. Figure 3 shows results of fracture mechanics for two strips of vacancies, with a varying angle between undefected sheet crack extension direction ( $Y$  axis) and direction of the strip of vacancies. For the highest angle (59 degrees), the crack does not follow the vacancy pattern. Instead, it propagates straight ahead similar as in the reference case shown in Figure 2. For the intermediate angle (30 degrees), the crack initially follows the direction of the vacancies, but eventually curves off and

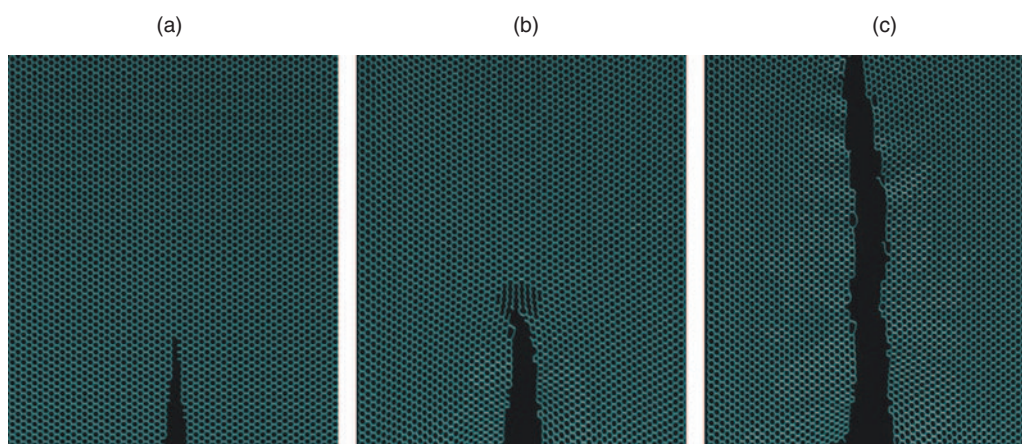


**Fig. 2.** Subplots (a–c) depict crack dynamics for the reference case, no vacancy defects present, under mode I loading as shown in Figure 1. The crack propagates straight through the crystal, leaving only slight angstrom scale surface roughness.

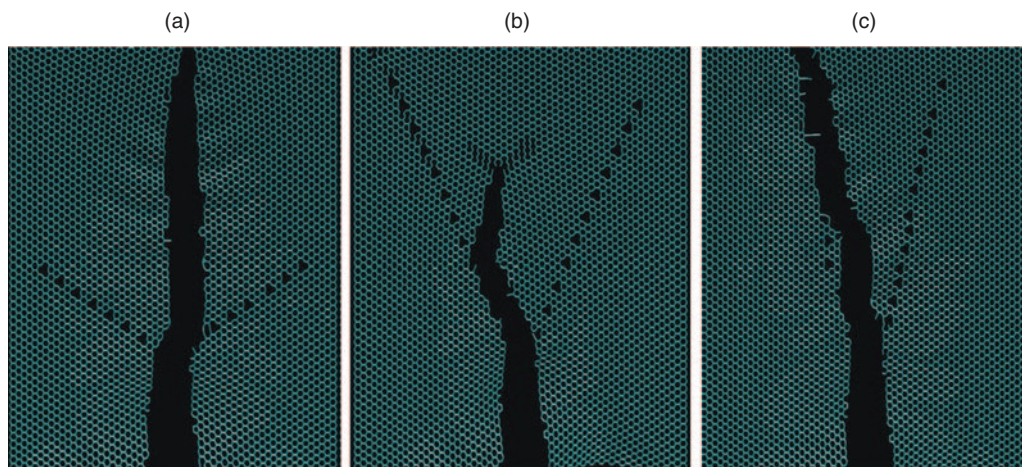


**Fig. 3.** Snapshots depict crack morphology snapshot for the case of straight vacancy strip patterns with 59 degree angle vacancies (subplot (a)), 30 degree angle vacancies (subplot (b)), and 13 degree vacancies (subplot (c)). The crack does not follow the vacancy pattern in the 59 degree case and follows only partly for the 30 degree case. For the 13 degree case, the crack follows the direction prescribed by the vacancy pattern.

propagates straight ahead. It is only for the smallest angle (13 degrees) that the crack follows the vacancy pattern direction through the entire simulation. Figure 4 depicts the dynamics of crack extension for the 30 degree and 13 degree cases, respectively. Overall, these results suggest that the direction of crack propagation could be controlled

by the choice of defect patterns, as long as the particular type of pattern falls within a small range of angle deviations from the undefected sheet propagation direction.

We now study a finer engineered vacancy pattern, in which a zig-zag defect pattern structure is considered. Figure 5 depicts the results of this study, showing that

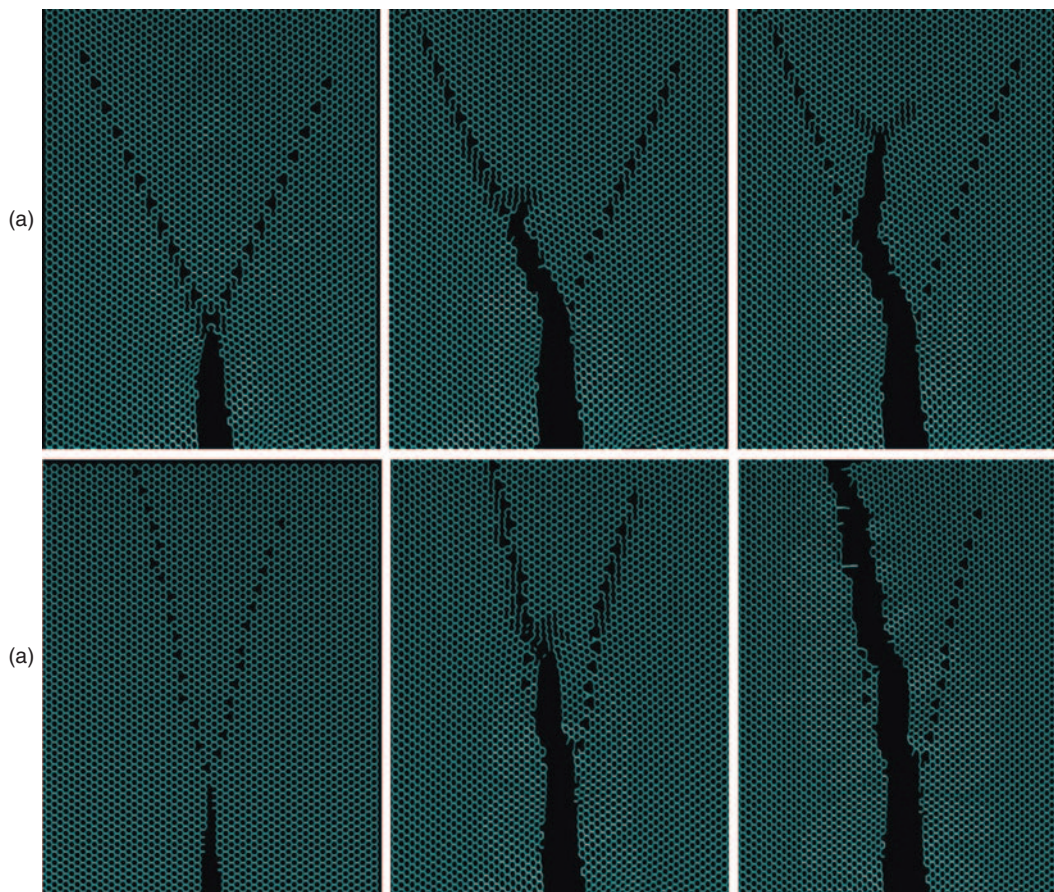


**Fig. 4.** Crack dynamics for two vacancy pattern angles, subplot (a) for 30 degree vacancies, and subplot (b) 13 degree vacancies. The angle is measured as the deviation of the vacancy pattern line from the  $+Y$  axis of undefected sheet crack growth. For the 30 degrees case, crack path follows the vacancy pattern to an extent, then deviates to  $+Y$  direction. For the 13 degree case, the crack follows the direction prescribed by the vacancy pattern until the entire slab is fractured.

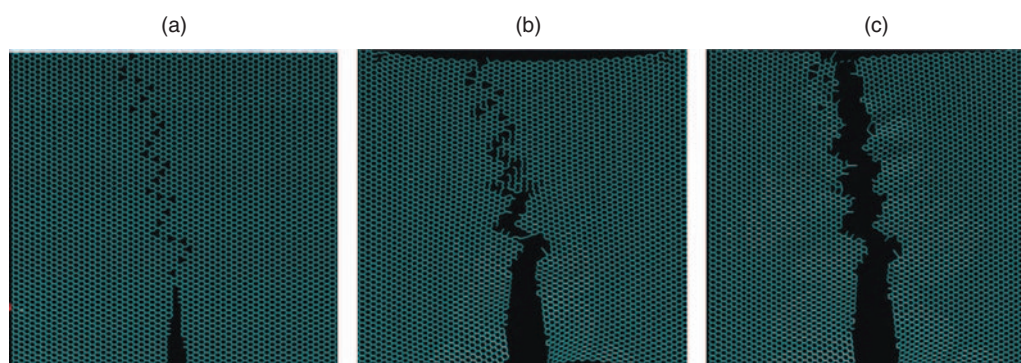


**Fig. 5.** Subplots (a–c) depict crack dynamics for the case of an engineered zig-zag pattern of vacancies. These snapshots illustrate that the crack follows the directions prescribed by the vacancy pattern, leading to the creation of two graphene nanosheets with a zig-zag surface structure. Slight deviation to this pattern is observed close to the edge of the slab, which is attributed to surface effects.

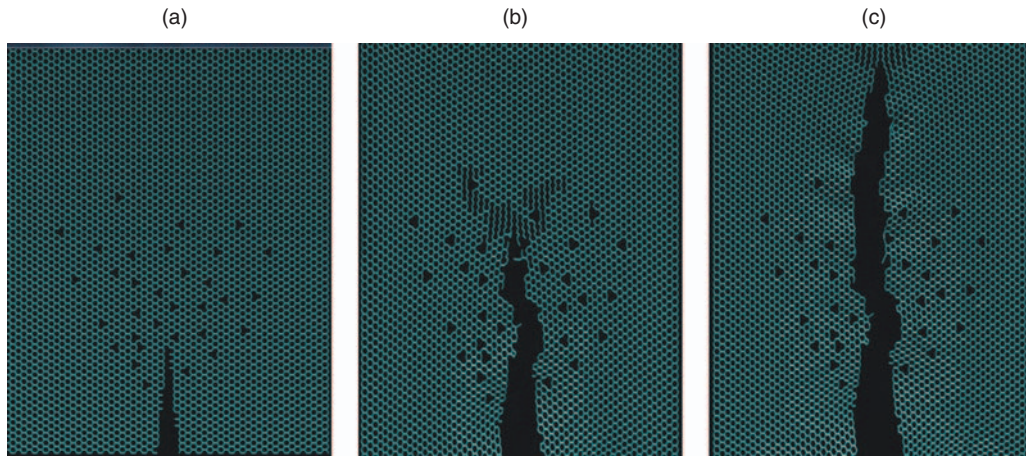


**Fig. 6.** Crack dynamics under the presence of randomly placed vacancies close to the tip of the crack (“vacancy cloud”). The crack is deflected from its initial straight path while it propagates through the cloud of vacancies.

the crack propagates along the direction of the prescribed weak paths, leaving behind a zig-zag surface geometry with structural features on the order of Angstroms to nanometers. This fracture behavior can be explained since the angles associated with this particular surface pattern structure are relatively small, so that the crack is able to follow the prescribed geometry.

Finally, we briefly review results for a random distribution of vacancy defects, as shown in Figure 6. It is observed that the crack is deflected randomly by the

presence of vacancies while propagating through the cloud of vacancies. However, it is again only affected by vacancies lying in a narrow band of angles from the  $Y$  direction. This method could be used to create random, more rough surface structures.

For all fracture runs we studied, the speed of fracture is of the order of  $\approx 4$  km/sec. Moreover, the presence of vacancies does not appear significantly affect the speed of fracture, as shown in Figure 7. Further, more detailed analyses of the fracture dynamics will be left to future investigations.

Figure 8 depicts the failure strain (applied strain) at which crack initiation occurs. For the no defect reference case, the failure strain is 5.3%. For the 13 degree angle it is slightly reduced to 4.85% (approximately 10% smaller), possibly due to the weakening of the graphene structure

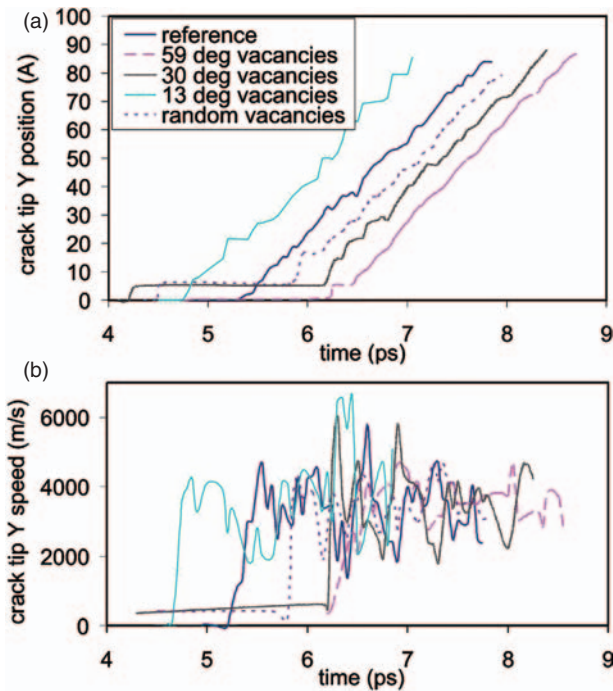


**Fig. 7.** Crack tip  $Y$  position versus time, for different vacancy geometries (subplot (a)), as well as crack speed as a function of time (subplot (b)). The crack tip speed, given by the slope of these curves, is seen not to be strongly affected by the presence of vacancies during the steady-state propagation regime. The zig-zag case is not included in this analysis.

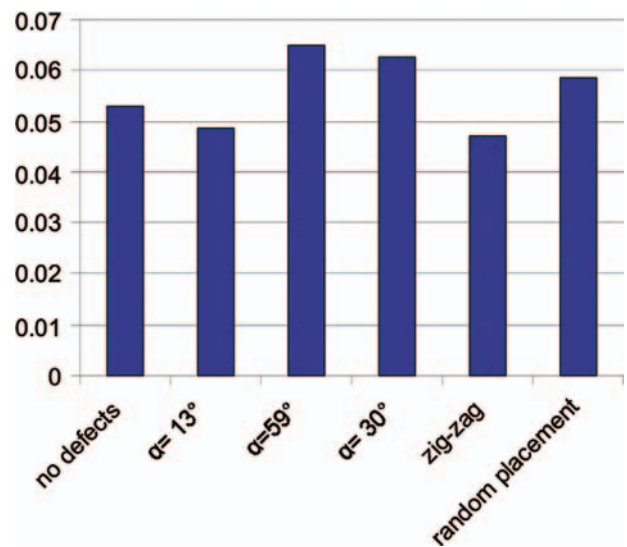


**Fig. 8.** Failure strain, for the different cases considered. The zig-zag and 13 degree angle cases show the lowest failure strains, whereas the high-angle patterns feature the largest failure strains.

under the presence of defects. For the 30 degrees and 59 degrees angles, the failure strain is increased to 6.5% and 6.25%, respectively (approximately 20% larger). This could be explained by a shielding effect in these geometries, caused by local shear along the 30/59 degree planes, which prevents perfectly brittle fracture to occur at lower strains. The zig-zag case (involving an initial vacancy line at 13 degrees) is similar to the 13 degree case, as expected. Random placement leads to a slight increase of failure strain to 5.85% (approximately 10% larger). This may also be explained by shielding effects, similar to the 30/59 degree cases.

#### 4. SUMMARY AND CONCLUSIONS

We have carried out systematic studies of the influence of patterns of vacancies in graphene on the dynamics of crack propagation. Our studies suggest that engineering vacancy structures ahead of a seed crack can be used to control the fracture behavior of graphene sheets, leading to distinct surface geometries. We find that there is a critical value of angular displacement beneath which the vacancy defect will redirect the crack path. This approach could be used to engineer a surface structure design following a zig-zag pattern, as it was illustrated in Figure 5. Overall, it is found that depending on the type of vacancy patterns studied, a distinct fracture behavior is observed.

Other defect patterns and associated crack dynamics could be investigated in future studies. Temperature effects can also play a significant role in guiding cracks along defect paths, and should be investigated for future studies. In particular, simulations at elevated temperatures could provide useful insight into experimental conditions. To the best of the author's knowledge, the study reported here is the first of its kind of applying the first principles based reactive force field ReaxFF to model fracture of graphene. ReaxFF is capable of describing a wide range of chemical elements and their interactions, including organics (e.g., H<sub>2</sub>) or metals (e.g., Ni, Cu). Thus the successful applicability of this force field to describe fracture of graphene may open novel applications, in particular those that involve chemically complex systems. For example, it could be applied to provide further analysis of the recently proposed approach to controlled nanocutting of graphene by using Ni nanoparticles.<sup>16</sup> Similarly, future work could include studying the effects of other atomistic defects such as doping the graphene sheets with nitrogen or oxygen atoms. Varying the conditions of temperature and displacement rate could provide other avenues of further investigation.

Additional study of this approach of graphene nanocutting via vacancy patterns should include

conducting experimental work with graphene sheets where vacancies are created by either by Atomic Force Microscopy or Scanning Tunneling Microscopy, for instance. We emphasize, however, that the focus of the present study was solely on a computational case study, and that major experimental challenges remain. These include the creation of vacancies at atomic-level precision and the application of tensile strain at ultra-small material length-scales.

**Acknowledgments:** The authors acknowledge support from ARO grant number W911NF-06-1-0291 (program manager Dr. Bruce LaMattina), as well as support from DARPA. Rhonda Jack acknowledges support from MIT's Summer Research Program (MSRP). All computations were carried out at MIT's Laboratory for Atomistic and Molecular Mechanics (LAMM).

#### References

1. J. C. Meyer et al., *Nature* 446, 60 (2007).
2. K. S. Novoselov et al., *Science* 306, 666 (2004).
3. A. Neto and E. Kim, Arxiv preprint cond-mat/0702562 (2007).
4. S. Dalosto and Z. Levine, Controlling the Band Gap in Zigzag Graphene Nanoribbons with an Electric Field Induced by a Polar Molecule.
5. Y. Zhang et al., *Nature* 438, 201 (2005).
6. R. Westervelt, *Science* 320, 324 (2008).
7. F. Schedin et al., *Nat. Mater* 6, 652 (2007).
8. P. Pandey, *Anal. Lett.* 41, 159 (2008).
9. P. Shemella et al., *Appl. Phys. Lett.* 91, 042101 (2007).
10. K. Novoselov et al., *Nature* 438, 197 (2005).
11. M. Han et al., *Phys. Rev. Lett.* 98, 206805 (2007).
12. Y. Son, M. Cohen, and S. Louie, *Phys. Rev. Lett.* 97, 216803 (2006).
13. B. Obradovic, et al., *Appl. Phys. Lett.* 88, 142102 (2006).
14. D. Jiang, B. Sumpster, and S. Dai, *The J. Chem. Phys.* 126, 134701 (2007).
15. Z. Chen et al., *Physica E: Low-Dimensional Systems and Nanostructures* 40, 228 (2007).
16. L. Ci et al., *Nano Research* 1, 116 (2008).
17. A. Tseng, *Optics and Laser Technology* 39, 514 (2007).
18. A. Omeltchenko et al., *Phys. Rev. Lett.* 78, 2148 (1997).
19. R. Khare et al., *Physical Review B* 75, 75412 (2007).
20. A. C. T. V. Duin et al., *J. Phys. Chem. A* 105, 9396 (2001).
21. K. D. Nielson et al., *J. Phys. Chem. A* 109, 49 (2005).
22. S. Han et al., *The J. Chem. Phys.* 123, 114703 (2005).
23. D. Sen et al., Direct atomistic simulation of brittle-to-ductile transition in silicon single crystals. in submission.
24. M. J. Buehler et al., *Phys. Rev. Lett.* 99, 165502 (2007).
25. M. J. Buehler, A. C. T. V. Duin, and W. A. Goddard, *Phys. Rev. Lett.* 96, 095505 (2006).
26. C. Xin, R. King, and M. J. Buehler, *Mat. Res. Soc. Proceedings* (2007).
27. W. Humphrey, A. Dalke, and K. Schulten, *Journal of Molecular Graphics* 14, 33 (1996).
28. Y. Ma et al., *Methods* 1.

Received: 9 October 2008. Accepted: 2 November 2008.